Slovak Society of Chemical Engineering
Institute of Chemical and Environmental Engineering
Slovak University of Technology in Bratislava

PROCEEDINGS

52nd International Conference of the Slovak Society of Chemical Engineering SSCHE 2026

Hotel SOREA TRIGAN
Štrbské Pleso, Slovakia
May 26 - 29, 2026

Editors: Assoc. prof. Mário Mihaľ

ISBN: 978-80-8208-177-3, EAN: 9788082081773

Published by the Faculty of Chemical and Food Technology, Slovak University of Technology in Bratislava in Slovak Chemistry Library for the Institute of Chemical and Environmental Engineering; Radlinského 9, 812 37 Bratislava, 2026

SERDAROĞLU, G.: The 2-phenylacetic acid derivatives functionalized with NH2 and -NO2 groups: FMO, NBO, UV-Vis, Pharmacokinetics studies, Editors: Mihaľ, M., In *52nd International Conference of the Slovak Society of Chemical Engineering SSCHE 2026*, Štrbské Pleso, Slovakia, 2026.

The 2-phenylacetic acid derivatives functionalized with $–NH_2$ and $-NO_2$ groups: FMO, NBO, UV-Vis, Pharmacokinetics studies

Goncagül Serdaroğlu

[1]*Sivas Cumhuriyet University, Faculty of Education, Math. and Sci. Edu., 58140, Sivas, Turkey; e-mail: goncagul.serdaroglu@gmail.com*

The phenyl-acetic acid (PAA), known as a natural auxin, is sourced mostly from fruits and has antimicrobial, antioxidant, and antifungal activities. Herein, the -NH2 and -NO2 groups were used to functionalize the PAA core structure, changing the positions of these groups. The effect on the reactivity, electronic spectra, and pharmacokinetics profiles of the substituent group and position on the PAA was investigated using computational tools. The geometry optimizations of the compounds were conducted at B3LYP/6-311++G** level, and then each of the structures was confirmed by no negative frequencies. The TD-DFT simulations were performed to elucidate the electronic spectra of the compounds. The NBO simulations were conducted to estimate and then evaluate the intramolecular interactions that contribute to decreasing stabilization energy. The FMO and MEP analyses were also performed to determine the global reactivity features and reactive site(s) of the compounds. The pharmacokinetics, drug-likeness, and bioavailability indexes were predicted using SwissADME tools.

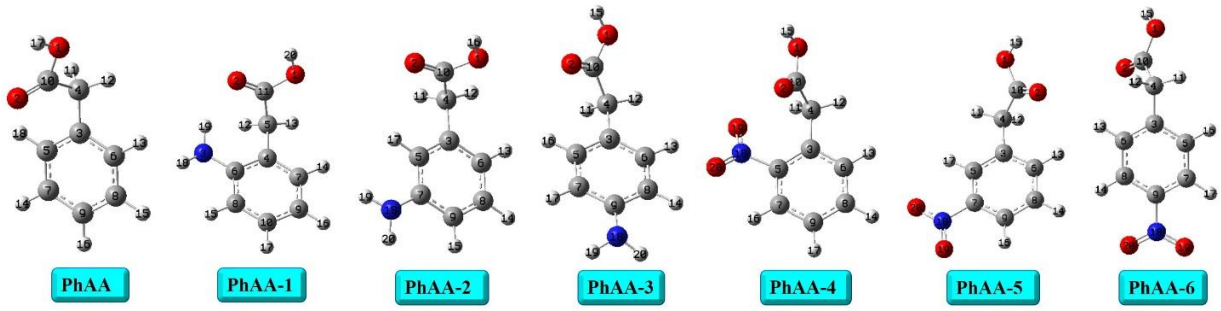

Key Words: *phenylacetic acid, UV-Vis, FMO, NBO, MEP, pharmacokinetics*

Acknowledgement: All calculations have been conducted at TUBITAK ULAKBIM, High Performance and Grid Computing Center (TR-Grid e-Infrastructure). The author thanks the Scientific Research Projects Department of Cumhuriyet University (Project No: EĞT-2023-098).

References

[1] Becke AD (1993) J Chem Phys. 98: 1372-1377.
[2] Lee C, Yang W, Parr RG (1988) Phys Rev B. 1988; 37: 785-789.
[3] Gaussian 16W, Revision D.01, Gaussian, Inc, Wallingford CT, 2016.
[4] Parr RG, Szentpaly LV, Liu S (1999) J Am Chem Soc 121: 1922-1924.
[5] Daina A, Michielin O, Zoete V (2017) Sci Rep 7(1): 1-13.

The 2-phenylacetic acid derivatives functionalized with $–NH_2$ and $–NO_2$ groups: FMO, NBO, UV-Vis, Pharmacokinetics studies

Goncagül Serdaroğlu

[1]*Sivas Cumhuriyet University, Faculty of Education, Math. and Sci. Edu., 58140, Sivas, Turkey; e-mail: goncagul.serdaroglu@gmail.com*

Keywords: *phenylacetic acid, UV-Vis, FMO, NBO, MEP, pharmacokinetics*

Abstract

The phenyl-acetic acid (PAA), known as a natural auxin, is sourced mostly from fruits and has antimicrobial, antioxidant, and antifungal activities. Herein, the $–NH_2$ and $–NO_2$ groups were used to functionalize the PAA core structure, changing the positions of these groups. The effect on the reactivity, electronic spectra, and pharmacokinetics profiles of the substituent group and position on the PAA was investigated using computational tools. The geometry optimizations of the compounds were conducted at B3LYP/6-311++G** level, and then each of the structures was confirmed by no negative frequencies. The TD-DFT simulations were performed to elucidate the electronic spectra of the compounds. The NBO simulations were conducted to estimate and then evaluate the intramolecular interactions that contribute to decreasing stabilization energy. The FMO and MEP analyses were also performed to determine the global reactivity features and reactive site(s) of the compounds. The pharmacokinetics, drug-likeness, and bioavailability indexes were predicted using SwissADME tools.

1. Introduction

Phenyl acetic acid (PAA) consists of a phenyl and a carboxylic acid group, and as a member of the phenylalanine-derived natural auxin, is naturally found in fruits and also obtained from the meta-pleural gland of most ant species [1,2]. PAA is responsible for the flavor of the honey and plays a critical role in the production of fragrances, insecticides, and cosmetic ingredients [3,4]. The PAA has been investigated in terms of its biological activity, such as antimicrobial, antifungal, antibacterial, etc [5-7]. On the other hand, the commerce of the PAA is under control in the world because it can be used illegally in the production of phenyl-acetone, which is used to produce amphetamines [8]. In the past, Samsonowicz has investigated the PAA and phenoxy-acetic acid using B3LYP/6-311++G** level simulations to elucidate the electronic (NBO and FMO) and spectroscopic (IR and NMR) behaviors and compare them with the benzoic acid [9]. Moreover, Srivastava and co-workers have reported the reactivity and acidic behaviors of the halogenated PAA structure at B3LYP/6-311++G** level [10].

Herein, the functionalized PAA core structure by the ortho-, meta-, and para-positioned $–NO_2$ and $–NH_2$ groups is investigated using in silico tools. The quantum mechanical computations of the designed structures are conducted at B3LYP/6-311++G** level to geometry optimizations, NBO, and FMO analyses in addition to the FT-IR and UV-Vis spectroscopic simulations. Moreover, the pharmacokinetics, druglikeness, and bioavailability are determined using SwissADME tools.

2. Computational Methods

2. 1. Quantum Mechanical Computations

All DFT and TD-DFT [11] of the PAA and its $–NH_2$ and $–NO_2$ substituted derivatives were done using the G16W [12] package, at B3LYP/6-311++G** level [13-15]. The simulated vibrational modes of the molecules were scaled by 0.96 (high-frequencies) and 0.988 (low-frequencies) to make them comparable with the observed counterparts [16]. The GaussView 6.0.16 [17] was used to analyze the FMOs and to illustrate the optimized geometries, UV spectra, and FMO& MEP plots of the compounds. The "*I*, ionization energy" and "*A*, electron affinity" values of the compounds is obtained from the energies of the HOMO and LUMO, depending on the Koopmans' theorem [18]. Then, the *I* and *A* values are used to determine the global reactivity values; $\chi \rightarrow$ "electronic chemical potential" $\eta \rightarrow$ "global hardness", $\omega \rightarrow$ "electrophilicity", $\Delta N_{max} \rightarrow$ "the maximum charge transfer capability index" [19-22], $\omega^- \rightarrow$ "the electrodonating power" and $\omega^+ \rightarrow$ "the electroaccepting power" [23], and $\Delta E_{back\text{-}donat.} \rightarrow$ "back-donation energy" [24]. The NBO analyses are performed to predict the essential intramolecular interactions which contribute to lowering the ($E^{(2)}$) (stabilization energy) [25,26].

2. 2. Pharmacokinetics and Drug-likeness

The lipophilicity values were predicted by using the five methods as follows: ILOGP [27], XLOGP [28], WLOGP [29], MLOGP [30], and SILICO-IT [31]. The water solubility scores of the compounds were estimated using three approaches: ESOL [32], ALI [33], and SILICO-IT [31]. The drug-likeness indexes were determined by using the five rules as follows: Lipinski [30], Ghose [34], Veber [35], Egan [36], and Muegge [37]. The physicochemical (see Table 1), pharmacokinetics, drug-likeness, and bioavailability [38] scores of the studied molecules were determined by SwissADME [39] tools.

Table 1. Physicochemical properties

	PhA	**PhA-1, PhA-2, PhA-3**	**PhA-4, PhA-5, PhA-6**
Formula	C8H8O2	C8H9NO2	C8H7NO4
MW (g/mol)	136.15	151.16	181.15
Num. HA	10	11	13
Num. AHA*	6	6	6
Fraction Csp3	0.12	0.12	0.12
Num. RB*	2	2	3
Num. HBA*	2	2	4
Num. HBD*	1	2	1
Molar Ref.	37.99	42.39	46.81
TPSA (Å²)*	37.30	63.32	83.12

*TPSA "topological polar surface Area"; HBA, "hydrogen bond acceptor"; HBD, "hydrogen bond donor"; RB, "rotatable bonds"; AHA, "aromatic heavy atoms"; Ref, "Refractivity".

3. Result and Discussion

3. 1. Molecular Geometry and Thermochemistry

The optimized structures of the PAA and its $–NH_2$ and $–NO_2$ substituted derivatives (and isomers) were illustrated in Fig.1. From Table 2, the ΔE, ΔH, and ΔG state functions of the main PAA molecule were determined at -460.115256, -460.105669, and -460.150939 au, respectively. Moreover, the ΔG values of the PAA-1-3 were determined at -515.511387, -515.509467, and -515.509203 au, respectively, which implied that the ortho-positioned $–NH_2$ group would gain more stability in PAA than the other positions. On the other hand, the para-positioned $–NO_2$ group functionalized PAA-6 would be more stable than the other would $–NO_2$ modified isomers. Namely, the free energy values (au) of the $–NO_2$ modified PAA isomers changed as follows: PAA-6 (-664.703163)

< PAA-5 (-664.708782) < PAA-4 (-664.703163). The thermal energies of the $–NH_2$ decorated PAA compounds were calculated to be greater than those of the $–NO_2$ modified counterparts. Namely, the $E_{therm.}$ values of the compounds were determined as PAA-1 (107.028) > PAA-2 (106.723)> PAA-3 (106.543) > PAA-4 (98.530) > PAA-5 (98.468) > PAA-6 (98.463). Furthermore, the PAA-5 (40.861 cal/mol.K) would have the biggest heat capacity among the compounds, and vice versa for PAA (32.294 cal/mol.K). The entropy value of the para-NO_2 substituted PAA-6 molecule was calculated at 109.220 cal/mol.K bigger than that of the other compounds. Also, the dipole moment (5.81 D) and polarizability (105.10 au) values of the PAA-6 would be greater than both the main structure and the $–NH_2$ substituted counterpart.

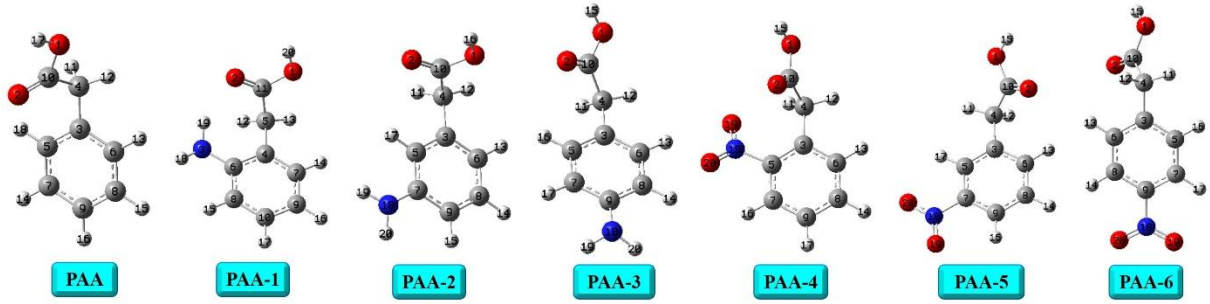

Fig. 1. The optimized structures

Table 2. The thermochemical and physical values

	ΔE (au)	ΔH (au)	ΔG (au)	$E_{therm.}$ (kcal/mol)	Cv (cal/mol.K)	S (cal/mol.K)	μ (D)	α (au)
PAA	-460.115256	-460.105669	-460.150939	95.274	32.294	95.278	1.34	87.67
PAA-1	-515.475965	-515.465429	-515.511387	107.028	37.354	96.727	0.80	97.71
PAA-2	-515.472295	-515.461270	-515.509467	106.723	38.218	101.439	1.50	98.10
PAA-3	-515.471715	-515.460621	-515.509203	106.543	38.382	102.249	2.12	99.09
PAA-4	-664.664741	-664.652848	-664.703163	98.530	40.715	105.899	4.44	102.54
PAA-5	-664.669151	-664.657070	-664.708782	98.468	40.861	108.837	4.70	104.01
PAA-6	-664.669100	-664.656996	-664.708890	98.463	40.850	109.220	5.81	105.10

3. 2. FT-IR Study

From Table 3, the peaks that appeared in the range of 3594-3608 cm^{-1} of the calculated IR spectra of the compounds were associated with the –OH elongation mode. For the PAA-1, PAA-2, and PAA-3 isomers, the asymmetric and symmetric νNH2 modes were assigned in the ranges of 3484-3518 and 3367-3424 cm^{-1}, respectively. The aliPAAtic –CH stretching modes of the compounds related to the –CH2 group were determined in the ranges of 2890-2995 cm^{-1}, whereas the νCH modes belonging to the aromatic ring of the compounds would be in the range of 3022-3097 cm^{-1}. The characteristic –C=O stretching for the compounds was estimated in the range of 1774-1814 cm^{-1} with a strong intensity. The simulated peaks at 1669, 1646, and 1650 cm^{-1} for the PAA-1, PAA-2, and PAA-3 isomers were associated with the scissoring mode (δNH2) of the –NH2 group. Moreover, the τNH2 mode for the PAA-1, PAA-2, and PAA-3 isomers was determined at 1162, 1169, and 1140 cm^{-1}, whereas the ωNH2 bending mode of these compounds would appear at the lower frequency region at 581, 599, and 651 cm^{-1}. On the other hand, the νN=O mode related to the –NO2 group of the PAA-4, PAA-5, and PAA-6 isomers was assigned in the range of 1581-1646 cm^{-1}, and was accompanied by the νCC and ipbHCC vibrations. The νCO mode related to the carboxyl group of the compounds was accompanied by both the twisting or wagging modes and the β HOC mode in the range of 1123- 1382 cm^{-1}.

Table 3. The calculated frequencies of the compounds in gas

Assignment	**PAA**	**PAA-1**	**PAA-2**	**PAA-3**	**PAA-4**	**PAA-5**	**PAA-6**
νOH	3602	3594	3600	3601	3608	3602	3601
νNH2 (asym.) (**PAA-(1-3))**	---	3484	3518	3514	---	---	---
νNH2 (sym) (**PAA-(1-3))**	---	3367	3424	3420	---	---	---
νCH	3064	3062	3056	3060	3096	3097	3097
νCH	3028	3023	3027	3022	3042	3056	3047
νCH2	2975	2995	2995	2973	2990	2980	2980
νCH2	2900	2924	2939	2890	2939	2904	2904
νC=O	1811	1774	1798	1809	1814	1810	1811
δNH2 (**PAA-(1-3))**	---	1669	1646	1650	---	---	---
δNH2 (**PAA-(1-3))**+ νCC+ ipbHCC/+νN=O (**PAA-(4-6))**	1630	1626	1627	1635	1640	1646	1635
νCC+ ipbHCC/ + νN=O (**PAA-(4-6))**	1609	1602	1610	1601	1604	1608	1624
νCC+ ipbHCC/ + νN=O (**PAA-(4-6))**	1513	1511	1511	1534	1581	1585	1578
νCC+ ipbHCC	1470	1476	1478	1457	1498	1499	1510
δCH2	1445	1461	1461	1443	1462	1460	1450
νCO+ τ/ ω CH2+ βHOC	1379	1374	1365	1378	1382	1379	1377
νNC+ ωCH2+βHOC	1320	1294	1311	1294	1364	1363	1363
νCO+ τCH2+ βHOC	1199	1225	1225	1202	1207	1200	1199
τNH2 (**PAA-(1-3))**+ βCCC	1168	1162	1169	1140	1174	1178	1189
νCO+ τCH2+ β HOC	1128	1127	1123	1124	1139	1134	1134
ipbHCC+ βCCC	1040	1049	964	1018	1058	1094	1022
opbHCC	989	960	954	948	997	993	981
ρCH2	948	940	928	919	944	962	947
β HOC+ βOCO (**PAA-(4-6))**	687	727	723	684	709	712	708
ωNH2 (**PAA-(1-3))**/ β HOC (**PAA-(4-6))**	648	581	599	651	657	671	689
βOCO+β HOC	515	509	487	487	509	483	517

***** The abbreviations are defined as: ν, stretching; β, bending; ipb, in-plane bending; opb, out-of-pane bending, δ, scissoring; τ, twisting; ω, wagging; ρ, rocking.

3. 3. UV-Vis Absorption Spectra

Table 4 and Fig. 2 presented the profiles of the electronic transitions and calculated UV spectra of the compounds, respectively. Accordingly, the first $s_0 \rightarrow s_1$ excitation for the PAA compound was determined at 231 nm (f= 0.0018) as a wide shoulder band, with the MO % contribution of H-1 → L (29.6), H-1 → L+1 (16.4), and H→L+1 (29.3). Also, the λ_{max} of the PhA molecule was predicted at 176 nm (*f*= 0.5093) due to the H-2→ L, H-1→ L+1, H-1→ L+2, and H→ L+1 transitions. Also, the first excitation for the PAA-1, PAA-2, and PAA-3 isomers was determined with the wavelength of 276, 274, and 268 nm, and slightly shifted to blue from the ortho to para- position of the $–NH_2$ group, due to the H→L transition. The simulated peaks at 313 nm for the PAA-5 and PAA-6 were due to the H-3→ L electronic transition, whereas the first excitation for the PAA-4 was contributed by both the H-3→ L (56.6% MO) and H→ L interactions (10.7%MO) at 318 nm. The $–NO_2$ and $–NH_2$ substitution on the aromatic ring of the PhA would cause the wavelength to shift to red. The calculated peaks would be due to the n→π* and π→π*.

Table 4. The theoretical UV-Vis absorption characteristics, in ethanol

Compound	***State***	Transitions	MO%	*ΔE (eV)*	*λ (nm)*	*f*
PAA	**1**	H-1→L H-1→L+1 H→L+1	(29.6%) (16.4%) (29.3%)	5.3844	231	0.0018
	9	H-2→L H-1→L+1 H-1→L+2 H→L+1	(27.2%) (8.4%) (12.1%) (20.1%)	7.0274	176	0.5093
PAA-1	**1**	H→L	(94.1%)	4.4882	276	0.0819

	4	H-1→L H-1→L+1 H-1→L+2 H→L+1	(33.3%) (17.2%) (9.0%) (13%)	5.7467	216	0.1475
	9	H-1→L+1 H-1→L+2 H→L+5	(32%) (20.3%) (14.8%)	6.5881	188	0.3244
PAA-2	**1**	H→L	(92.3%)	4.5296	274	0.0543
	4	H-1→L H-1→L+1 H→L+2	(5.9%) (19.2%) (28%)	5.6949	218	0.1890
	7	H-3→L H-1→L+1	(6.2%) (43.1%)	6.3877	194	0.2890
PAA-3	**1**	H→L	(91.3%)	4.6325	268	0.0414
	3	H→L+2	(71.7%)	5.4844	226	0.2749
	10	H-1→L	(41.8%)	6.6590	186	0.5836
PAA-4	**1**	H-3→L H→L	(56.6%) (10.7%)	3.8966	318	0.0198
	5	H-2→L	(42.4%)	4.6573	266	0.1033
	9	H→L+1	(62.8%)	6.2492	198	0.1246
PAA-5	**1**	H-3→L	(97.4%)	3.9555	313	0.0000
	2	H→L	(94.6%)	4.0560	306	0.0216
	4	H-1→L	(94.5%)	4.5092	275	0.2453
	9	H-2→L+1 H-1→L+2 H→L+1	(14.1%) (7.2%) (66.3%)	6.2245	199	0.1992
PAA-6	**1**	H-3→L	(97.4%)	3.9567	313	0.0000
	3	H-1→L H→L	(44%) (36.8%)	4.4111	281	0.2585
	9	H-5→L	(87.5%)	6.2852	197	0.0554

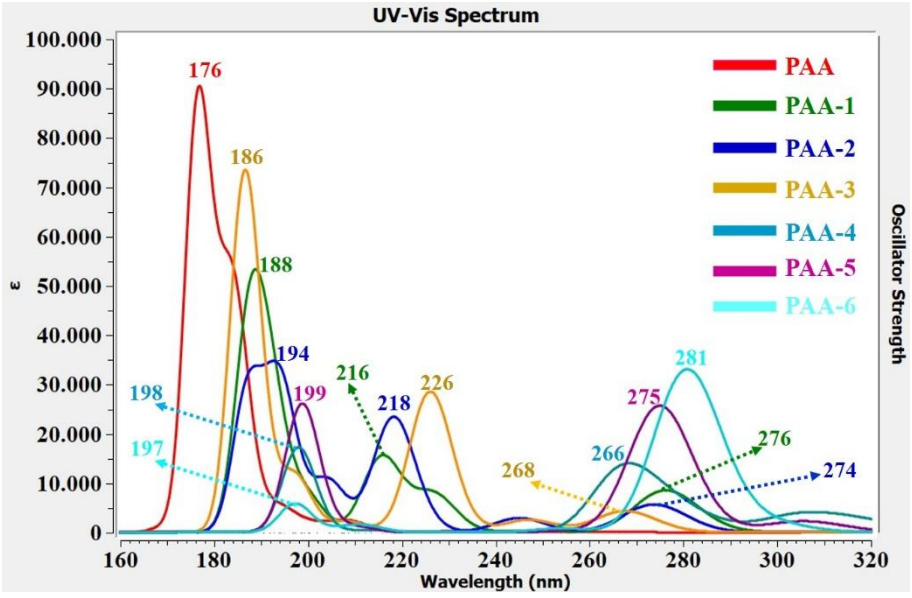

Fig. 2. The simulated UV-Vis spectra

3. 4. NBO Study

The important resonance and anomeric interactions and their energies of the PAA and its derivatives were summarized in Table 5. The LP (2) O1 (EDi= 1.82328e) → π* O2-C10 (EDj= 0.20558e) resonance interaction was determined with the $E^{(2)}$ of 42.75kcal/mol, which would contribute to lowering stabilization energy highly. Also, the $E^{(2)}$ values of the anomeric interactions LP (2) O2 → σ* O1-C10 and LP (2) O2 → σ* O4-C10 were determined at 32.93 and 19.71 kcal/mol; all these charge movements from the lone pairs of the Os to the unfilled molecular orbitals implied the remarkable electron delocalization on the carboxyl group. For the PAA-1, PAA-2, and PAA-3 isomers, the charge movement from the lone pair of the N atom to antibonding molecular orbitals of the phenyl ring would be important resonances that contributed to the lowering of $E^{(2)}$ predicted at 25.92, 27.47, and 26.47 kcal/mol, respectively. On the other hand, the anomeric interactions related to the $–NO_2$ group for the PAA-4 were determined with the $E^{(2)}$ of 18.74 and 18.95 kcal/mol, respectively, for LP (2) O19 → σ* N18-O20 and LP (2) O20 → σ* N18-O19 interactions. Also, the energy of the π C5-C7 → π* N18-O20 for the PAA-4 would be at 23.91 kcal/mol, whereas the similar interaction for the PAA-5 and PAA-6 was determined with the $E^{(2)}$ of 23.58 and 26.58 kcal/mol, respectively. The $–NH_2$ and $–NO_2$ groups would provide the additional electron delocalization(s) on the core structure, which affect the electron density on the surface of the PAA.

Table 5. NBO analysis results of the selected compounds, at B3LYP/6-311++G(d,p) in gas

Donor(i)	ED_i/e	Acceptor(j)	ED_j/e	$E^{(2)}$ kcal/mol	E(j)-E(i)/a.u	F(i.j)/a.u
PAA						
π C3-C6	1.66662	π* C5-C7	0.31630	19.75	0.29	0.068
		π* C8-C9	0.32969	20.68	0.28	0.069
π C5-C7	1.66333	π* C3-C6	0.34982	21.30	0.28	0.070
		π* C8-C9	0.32969	20.65	0.28	0.068
π C8-C9	1.66938	π* C3-C6	0.34982	20.15	0.29	0.068
		π* C5-C7	0.31630	20.08	0.29	0.068
LP (2) O1	1.82328	π* O2-C10	0.20558	42.75	0.36	0.111
LP (2) O2	1.83925	σ* O1-C10	0.10106	32.93	0.61	0.129
		σ* C4-C10	0.06992	19.71	0.63	0.102
PAA-1						
π C4-C6	1.61662	π* C7-C9	0.35942	24.39	0.29	0.075
		π* C8-C10	0.34712	16.97	0.28	0.063
π C7-C9	1.68113	π* C4-C6	0.42608	17.75	0.28	0.065
		π* C8-C10	0.34712	22.87	0.28	0.072
π C8-C10	1.70747	π* C4-C6	0.42608	21.91	0.28	0.073
		π* C7-C9	0.35942	16.80	0.29	0.063
LP (2) O1	1.81133	π* O2-C11	0.21280	41.41	0.37	0.112
LP (2) O2	1.84856	σ* O1-C11	0.09538	31.43	0.63	0.127
		σ* C5-C11	0.06222	16.99	0.65	0.096
LP (1) N3	1.83442	π* C4-C6	0.42608	25.92	0.33	0.088
PAA-2						
π C3-C6	1.67770	π* C5-C7	0.39451	16.73	0.28	0.062
		π* C8-C9	0.34206	23.44	0.28	0.073
π C5-C7	1.63490	π* C3-C6	0.38208	25.43	0.29	0.077
		π* C8-C9	0.34206	16.61	0.28	0.062
π C8-C9	1.71401	π* C3-C6	0.38208	16.07	0.29	0.062
		π* C5-C7	0.39451	22.20	0.28	0.073
LP (2) O1	1.81755	π* O2-C10	0.20772	44.91	0.35	0.113
LP (2) O2	1.84469	σ* O1-C10	0.10155	32.53	0.62	0.128
		σ* C4-C10	0.06373	18.64	0.64	0.100
LP (1) N18	1.84335	π* C5-C7	0.39451	27.47	0.33	0.090
PAA-3						

π C3-C6	1.68000	π* C5-C7	0.32937	22.77	0.28	0.072
		π* C8-C9	0.40229	17.27	0.28	0.063
π C5-C7	1.70942	π* C3-C6	0.37677	17.11	0.29	0.064
		π* C8-C9	0.40229	22.47	0.28	0.073
π C8-C9	1.63937	π* C3-C6	0.37677	23.99	0.29	0.075
		π* C5-C7	0.32937	16.40	0.29	0.062
LP (2) O1	1.82382	π* O2-C10	0.20456	42.09	0.36	0.111
LP (2) O2	1.83966	σ* O1-C10	0.10164	32.97	0.61	0.129
		σ* C4-C10	0.07008	19.40	0.64	0.101
LP (1) N18	1.84775	π* C8-C9	0.40229	26.47	0.33	0.090
PAA-4						
π C3-C6	1.64384	π* C5-C7	0.36744	19.83	0.28	0.067
		π* C8-C9	0.31869	21.78	0.28	0.071
π C5-C7	1.65004	π* C3-C6	0.32185	21.50	0.30	0.072
		π* C8-C9	0.31869	17.54	0.29	0.065
		π* N18-O20	0.60732	22.82	0.15	0.056
π C8-C9	1.63820	π* C3-C6	0.32185	19.27	0.29	0.067
		π* C5-C7	0.36744	23.91	0.28	0.073
π N18-O20	1.98691	LP (3) O19	1.45062	12.45	0.18	0.079
LP (2) O1	1.82212	π* O2-C10	0.20987	45.56	0.35	0.113
LP (2) O2	1.84062	σ* O1-C10	0.09886	32.73	0.62	0.129
		σ* C4-C10	0.07154	20.59	0.63	0.104
LP (2) O19	1.89964	σ* C5-N18	0.10803	12.55	0.56	0.075
		σ* N18-O20	0.05626	18.74	0.73	0.106
LP (2) O20	1.89406	σ* C5-N18	0.10803	13.94	0.56	0.079
		σ* N18-O19	0.05937	18.95	0.72	0.105
PAA-5						
π C3-C5	1.65044	π* C6-C8	0.30051	20.49	0.29	0.070
		π* C7-C9	0.37414	20.73	0.28	0.068
π C6-C8	1.63757	π* C3-C5	0.31635	19.51	0.29	0.067
		π* C7-C9	0.37414	23.58	0.28	0.072
		π* C3-C5	0.31635	20.78	0.30	0.071
π C7-C9	1.65362	π* C6-C8	0.30051	17.01	0.30	0.064
		π* N18-O19	0.62130	23.58	0.15	0.057
π N18-O19	1.98643	LP (3) O20	1.44499	12.51	0.18	0.079
LP (2) O1	1.81959	π* O2-C10	0.20875	44.18	0.35	0.112
LP (2) O2	1.83923	σ* O1-C10	0.09853	32.45	0.62	0.129
		σ* C4-C10	0.07002	20.02	0.63	0.103
LP (2) O19	1.89781	σ* C7-N18	0.11011	13.48	0.56	0.078
		σ* N18-O20	0.05558	18.80	0.73	0.105
LP (2) O20	1.89832	σ* C7-N18	0.11011	13.42	0.56	0.078
		σ* N18-O19	0.05505	18.71	0.73	0.105
PAA-6						
π C3-C5	1.63966	π* C6-C8	0.28516	17.86	0.29	0.065
		π* C7-C9	0.37537	23.63	0.28	0.073
π C6-C8	1.64602	π* C3-C5	0.33591	22.34	0.28	0.072
		π* C7-C9	0.37537	20.73	0.28	0.068
		π* C3-C5	0.33591	17.78	0.30	0.065
π C7-C9	1.65235	π* C6-C8	0.28516	20.01	0.30	0.071
		π* N18-O20	0.62266	26.58	0.15	0.061
π N18-O20	1.98621	LP (3) O19	1.44430	12.52	0.18	0.079
LP (2) O1	1.81984	π* O2-C10	0.20762	43.70	0.35	0.112
LP (2) O2	1.83861	σ* O1-C10	0.09895	32.54	0.62	0.129
		σ* C4-C10	0.07038	20.17	0.63	0.103
LP (2) O19	1.89823	σ* C9-N18	0.11019	13.41	0.56	0.078
		σ* N18-O20	0.05533	18.74	0.73	0.105
LP (2) O20	1.89816	σ* C9-N18	0.11019	13.43	0.56	0.078
		σ* N18-O19	0.05550	18.78	0.73	0.105

3. 5. Lipophilicity and water solubility

According to the WLOGP methods, the $–NO_2$ group increases the lipophilicity of the PAA core, while the $–NH_2$ decreases the lipophilic character. Namely, the WLOGP order of the compounds was determined as PAA-(4-6) (1.75) > PAA (1.31)> PAA- (1-3) (0.90), indicating that lipophilicity would not be affected by the position of the functional groups. Moreover, the substituent group position would not affect the lipophilicity depending on the MLOGP and SILICOS-IT methods, which both revealed the LOGP order as PAA > PAA-(1-3)> PAA- (4-6): both $–NO_2$ and $–NH_2$ groups decrease the lipophilicity of the core PAA structure. From Table 6, the LOGP behavior of the compounds depicted different directions depending on the method. According to the averaged LOGP values of the compounds, the PAA would be the most lipophilic molecule, while the PAA-1 would behave as the least lipophilic molecule, among the structures, with the Avg. $LogP_{o/w}$ order of PAA (1.43)> PAA-2 (0.95)> PAA-3 (0.92)> PAA-4 (0.91)> PAA-5 (0.87)> PAA-6 (0.86)> PAA-1 (0.66). The PAA-1 structure would be more soluble than the other structures, depending on the ESOL and Ali methods. Moreover, the PAA and $–NH_2$ functionalized PAA isomers would behave more soluble than those of the $–NO_2$ modified PAA isomers, depending on the Ali method. Namely, the solubility (mg/mL) of the structures was determined as PAA-1> PAA> PAA-3> PAA-2> PAA-6> PAA-5> PAA-4; PAA-1 would be the most hydrophilic molecule among the structures, and vice versa for PAA-4. On the other hand, the SILICO-IT method revealed the solubility (mg/mL) order of the compounds as PAA-(1-3)> PAA-(4-6)> PAA, and all compounds would be in the range of the "soluble" limit.

Table 6. Lipophilicity and water solubility

	PAA	**PAA-1**	**PAA-2**	**PAA-3**	**PAA-4**	**PAA-5**	**PAA-6**
Lipophilicity							
iLOGP	1.23	0.80	0.98	0.89	0.95	0.89	0.86
XLOGP3	1.41	-0.25	1.00	0.94	1.59	1.45	1.39
WLOGP	1.31	0.90	0.90	0.90	1.75	1.75	1.75
MLOGP	1.66	1.05	1.05	1.05	0.49	0.49	0.49
SILICOS-IT	1.54	0.82	0.82	0.82	-0.20	-0.20	-0.20
Avg. LogPo/w	1.43	0.66	0.95	0.92	0.91	0.87	0.86
Water Solubility							
Log S (ESOL)	-1.88	-0.89	-1.68	-1.64	-2.11	-2.02	-1.98
Solubility (mg/mL)	1.78	19.4	3.17	3.45	1.41	1.73	1.89
Class	VS	VS	VS	VS	S	S	VS
Log S (Ali)	-1.80	-0.62	-1.92	-1.86	-2.95	-2.80	-2.74
Solubility (mg/mL)	2.17	36.1	1.82	2.10	0.205	0.286	0.330
Class	VS	VS	VS	VS	S	S	S
Log S (SILICOS-IT)	-2.14	-1.80	-1.80	-1.80	-2.03	-2.03	-2.03
Solubility (mg/mL)	0.977	2.40	2.40	2.40	1.68	1.68	1.68
Class	S	S	S	S	S	S	S

*The abbreviations are defined as S, Soluble; VS, very soluble.

3. 6. Pharmacokinetics Profiles

The predicted GI absorption values of the compounds implied that all compounds would be highly capable of absorption by the GI tract because all compounds appeared in the white region of the BOILED-Egg. On the other hand, only the PAA compound would be capable of permeating via the BBB passively and appeared on the yolk-region of the BOILED-Egg model (Fig. 3). None of the compounds could have potency for the CYP1A2, CYP2C19, CYP2C9, CYP2D6, and CYP3A4 inhibitors. The PAA (-6.13 cm/s) core structure would be more capable of skin permeation, while the PAA-1 (-7.40 cm/s) could have less potency for skin permeation (Table 7).

In terms of the Log *Kp*, all compounds should be enriched structurally because it was calculated out of the optimum range [40] of (-2.3)-(6.8). According to the Lipinski, Veber, and Egan rules (Table 8), all compounds could meet the drug-likeness criteria, while the molecular weight of the structures (MW<200) was the reason for the violation of drug-likeness, depending on the Muegge approach. Moreover, the $–NO_2$ functionalized PAA isomers, depending on the Ghose rules, would meet the requested structural/physicochemical properties for drug-likeness, while $–NH_2$ substituted isomers (MW<160) would not meet the molecular-weight criteria.

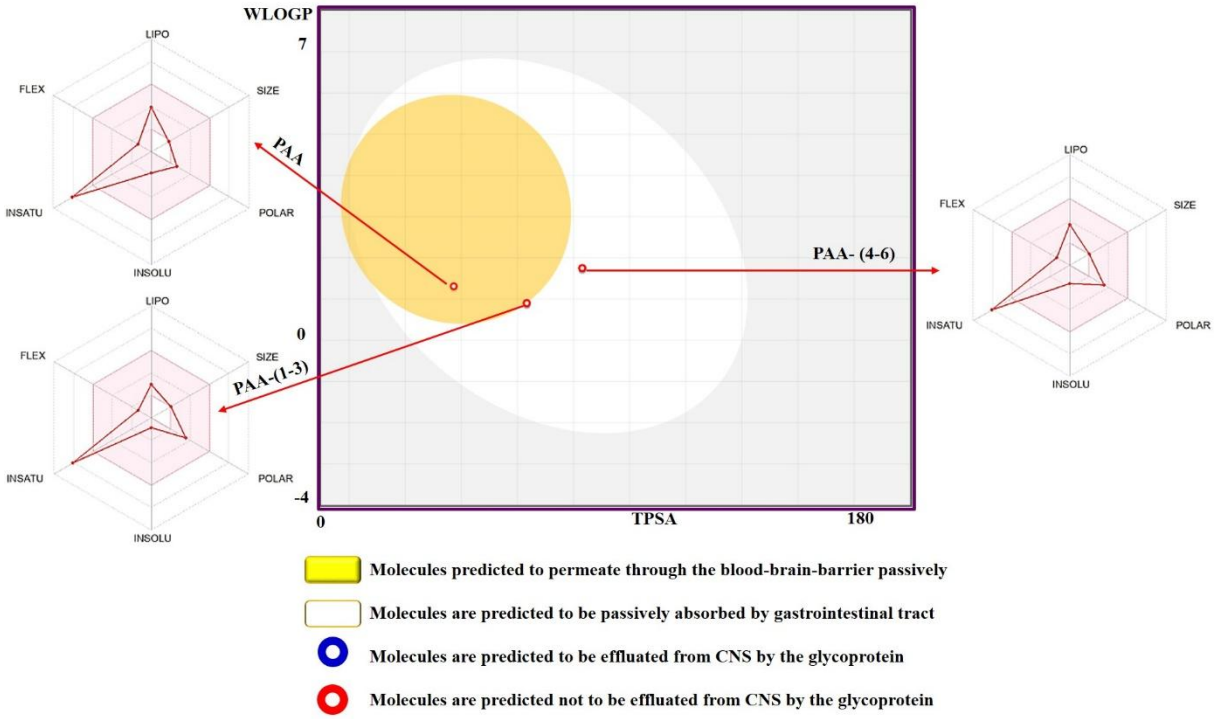

Fig. 3. BOILED-Egg model and radar graphs.

Table 7. Pharmacokinetics of the studied compounds

	PAA	**PAA-1**	**PAA-2**	**PAA-3**	**PAA-4**	**PAA-5**	**PAA-6**
GI absorption	High	High	High	High	High	High	High
BBB permeant	Yes	No	No	No	No	No	No
P-gp substrate	No	No	No	No	No	No	No
CYP1A2 inhibitor	No	No	No	No	No	No	No
CYP2C19 inhibitor	No	No	No	No	No	No	No
CYP2C9 inhibitor	No	No	No	No	No	No	No
CYP2D6 inhibitor	No	No	No	No	No	No	No
CYP3A4 inhibitor	No	No	No	No	No	No	No
Log K_p (skin permeation)/ cm/s	-6.13	-7.40	-6.51	-6.55	-6.28	-6.38	-6.42

Table 8. Drug-likeness and bioavailability values

	PAA	**PAA-1**	**PAA-2**	**PAA-3**	**PAA-4**	**PAA-5**	**PAA-6**
Lipinski	Yes	Yes	Yes	Yes	Yes	Yes	Yes
Ghose	No; MW<160,	No; MW<160	No; MW<160	No; MW<160	Yes	Yes	Yes

	MR<40, #atoms<20						
Veber	Yes	Yes	Yes	Yes	Yes	Yes	Yes
Egan	Yes	Yes	Yes	Yes	Yes	Yes	Yes
Muegge	No; MW<200	No; MW<200	No; MW<200	No; MW<200	No; MW<200	No; MW<200	No; MW<200
Bioavail.	0.85	0.85	0.85	0.85	0.56	0.56	0.56

3. 7. FMO and MEP Study

Herein, Table 9 presents the global reactivity parameters of the compounds. Accordingly, the HOMO energy order, PAA-3 (−5.585) > PAA-1 (−5.646) > PAA-2 (−5.699) > PAA (−6.855) > PAA-4 (−7.630) > PAA-5 (−7.642) > PAA-6 (−7.729), of the compounds implied that $–NH_2$ functional group could cause an increase in the HOMO energy of the PAA core, while the $–NO_2$ group could decrease the LUMO energy of the PAA core. On the other hand, the para-NH_2-positioned PAA-3 compound would have the highest LUMO energy, while the PAA-5 would have the lowest LUMO energy, that is, the LUMO order of the compounds was determined as PAA-3 (−0.198) > PAA (−0.412) > PAA-2 (−0.433) > PAA-1 (−0.482) > PAA-4 (−2.561) > PAA-6 (−2.587) > PAA-5 (−2.611). Then, the global reactivity parameters changed in the following orders:

ΔE (eV): PAA (6.443) > PAA-3 (5.388) > PAA-2 (5.266) > PAA-1 (5.164) > PAA-6 (5.142) > PAA-4 (5.068) > PAA-5 (5.031)

χ (eV): PAA-3 (−2.891) > PAA-1 (−3.064) > PAA-2 (−3.066) > PAA (−3.634) > PAA-4 (−5.095) > PAA-5 (−5.126) > PAA-6 (−5.158)

η (eV): PAA (3.222) > PAA-3 (2.694) > PAA-2 (2.633) > PAA-1 (2.582) > PAA-6 (2.571) > PAA-4 (2.534) > PAA-5 (2.516)

ω (eV): PAA-5 (0.192) > PAA-6 (0.190) > PAA-4 (0.188) > PAA (0.075) > PAA-1 (0.067) > PAA-2 (0.066) > PAA-3 (0.057)

ω^+ (au): PAA-5 (0.109) > PAA-6 (0.107) > PAA-4 (0.106) > PAA (0.023) > PAA-1 (0.022) > PAA-2 (0.021) > PAA-3 (0.016)

ω^- (au): PAA-5 (0.298) > PAA-6 (0.297) > PAA-4 (0.294) > PAA (0.157) > PAA-1 (0.135) > PAA-2 (0.134) > PAA-3 (0.123)

ΔN_{max} (eV): PAA-5 (2.038) > PAA-4 (2.011) > PAA-6 (2.006) > PAA-1 (1.187) > PAA-2 (1.164) > PAA (1.128) > PAA-3 (1.073)

$\Delta E_{back\text{-}donat}$ (eV): PAA-5 (−0.629) > PAA-4 (−0.634) > PAA-6 (−0.643) > PAA-1 (−0.645) > PAA-2 (−0.658) > PAA-3 (−0.673) > PAA (−0.805)

The PAA core would prefer the intermolecular interactions more than the intramolecular interactions due to the biggest energy gap value, and vice versa for the PAA-5. Moreover, the PAA would be determined as the hardest compound, whereas the PAA-5 would be the softest compound among the molecules. The electrophilicity indexes implied that the PAA-5 could be more electrophilic, and PAA-3 would be the least electrophilic compound. Also, the PAA-5 would have more electro-accepting and electro-donating potency, and vice versa for PAA-3. The PAA-5 would have more charge transfer capability than the others would, and vice versa for PAA-3. Lastly, the PAA could gain more stability via back-donation, while the PAA-5 would gain less stability. From Fig. 4, the HOMO of the PAA core was expanded on the whole surface, while the LUMO appeared on the phenyl ring, not on the carboxyl group. Moreover, the HOMO of the PAA-1 and PAA-3 separated on the carboxyl group in addition to the phenyl ring, whereas the HOMO of the PAA-2 would not be seen on the carboxyl group. On the

other hand, the LUMO for PAA-1 and PAA-2 would be expanded on the whole surface, while the LUMO of the PAA-3 would not be expanded on the carboxyl group in addition to the $–NH_2$ group. For the PAA-(4-6) isomers, the HOMO would be distributed on the $–NO_2$ group for all compounds and the phenyl ring for the PAA-4. The MEP plots indicated that the H atom of the -OH group would be sensitive to the nucleophilic attacks because this H was covered by the blue color as an indicator of the electron-poor region (V>0). Also, the carbonyl group's O atom for all compounds was covered by the red color as a marker of the electron-rich region (V<0) for the electrophilic attacks.

Table 9. The chemical reactivity parameters

	PAA	PAA-1	PAA-2	PAA-3	PAA-4	PAA-5	PAA-6
H (-I) (eV)	-6.855	-5.646	-5.699	-5.585	-7.630	-7.642	-7.729
L (-A) (eV)	-0.412	-0.482	-0.433	-0.198	-2.561	-2.611	-2.587
ΔE (eV)	6.443	5.164	5.266	5.388	5.068	5.031	5.142
χ (eV)	-3.634	-3.064	-3.066	-2.891	-5.095	-5.126	-5.158
η (eV)	3.222	2.582	2.633	2.694	2.534	2.516	2.571
ω (eV)	0.075	0.067	0.066	0.057	0.188	0.192	0.190
ω^+ (au)	0.023	0.022	0.021	0.016	0.106	0.109	0.107
ω^- (au)	0.157	0.135	0.134	0.123	0.294	0.298	0.297
ΔN_{max} (eV)	1.128	1.187	1.164	1.073	2.011	2.038	2.006
$\Delta\varepsilon_{back\text{-}donat.}$ (eV)	-0.805	-0.645	-0.658	-0.673	-0.634	-0.629	-0.643

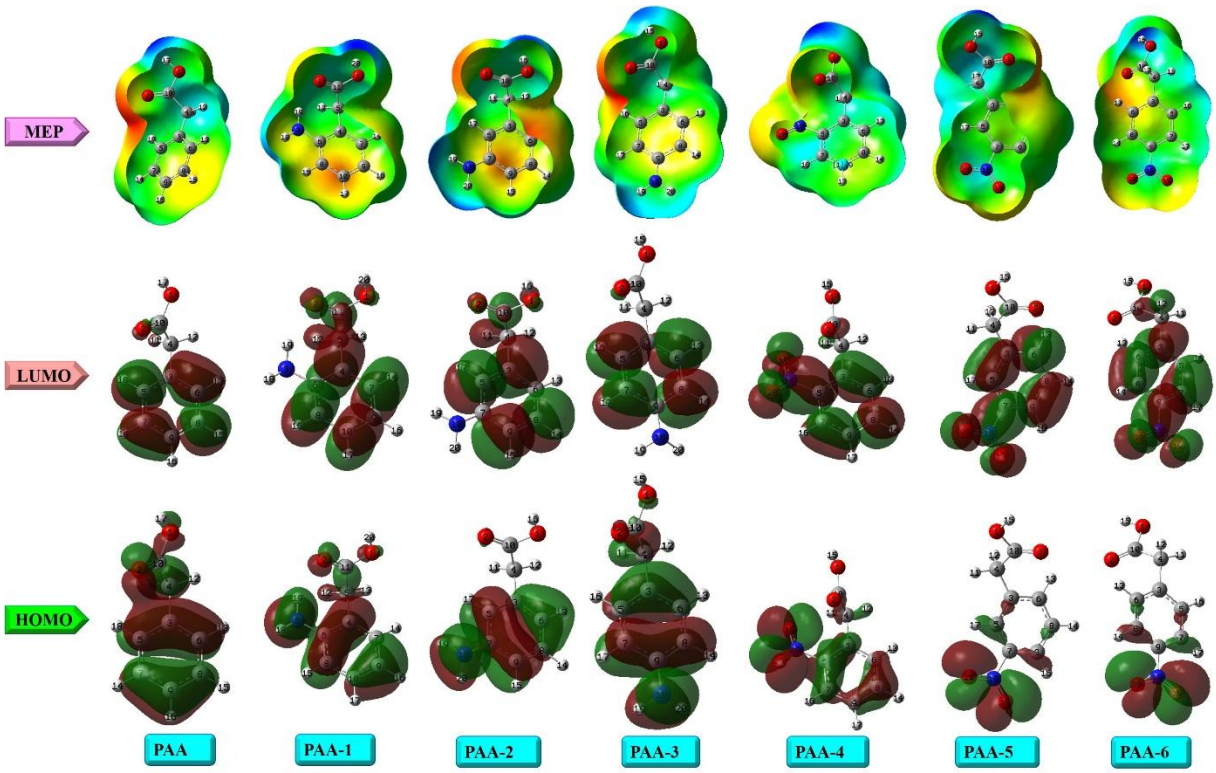

Fig. 4. HOMO& LUMO (isoval:0.02), and MEP (isoval:0.0004) graphs

4. Conclusions

In this work, the DFT and TD-DFT simulations were performed to evaluate the thermochemical, electronic, and spectroscopic properties of the PAA and $–NH_2$ and $–NO_2$ substituted isomers of PAA. The dipole moment (5.81 D) and polarizability (105.10 au) values of the PAA-6 would be greater than both the main structure and the $–NH_2$

substituted counterpart. Also, the para-NO_2 substituted PAA-6 molecule would have the highest entropy value at 109.220 cal/mol.K, among the compounds. The UV-Vis works revealed that the $–NO_2$ and $–NH_2$ substitution on the aromatic ring of the PhA would cause the wavelength to shift to red, and the calculated peaks would be due to the $n\rightarrow\pi^*$ and $\pi\rightarrow\pi^*$. Moreover, the $–NH_2$ and $–NO_2$ groups would provide the additional electron delocalization(s) on the core structure, which affects the electron density on the surface of the PAA, based on the results of the NBO. The MEP plots implied that the H atom of the -OH group would be sensitive to the nucleophilic attacks, whereas the carbonyl group's O atom for all compounds was covered by the red color as a marker of the electron-rich region ($V<0$) for the electrophilic attacks.

Acknowledgments

All calculations have been carried out at TUBITAK ULAKBIM, High Performance and Grid Computing Center (TR-Grid e-Infrastructure). The author thanks the Scientific Research Projects Department of Sivas Cumhuriyet University (Project No: EĞT-2023-098).

References

[1] Cook SD (2019) An historical review of phenylacetic acid. Plant Cell Physiol 60(2):243–254.

[2] Perez VC, Zhao H, Lin M, Kim J (2023) Occurrence, function, and biosynthesis of the natural auxin phenylacetic acid (PAA) in plants. Plants 12(2):266.

[3] Serra Bonvehí J, Ventura Coll F (2003) Flavour index and aroma profiles of fresh and processed honeys. J Sci Food Agric 83(4):275–282.

[4] Liao Z, Parumasivam T, Xiao Z, Zhu X, Yeoh YK, Ye X, Tan TC (2026) Emerging therapeutic and cosmeceutical applications of phenylalanine and its metabolites. Cutan Ocul Toxicol 1–18.

[5] Mani-López E, Mejía-Garibay B, Hernández-Figueroa RH, López-Malo A (2026) Phenyllactic acid from lactic acid bacteria: a natural antimicrobial for food biopreservation. Fermentation 12(4):184.

[6] Oufensou S, Fabbri D, Dettori MA, Carta P, Azara E, Ugone V, Migheli Q (2026) Evaluation of antifungal and antimycotoxigenic activity of selected natural antioxidants against Fusarium culmorum: in vitro and in planta assays. J Sci Food Agric. 106(7):4417-4425

[7] Xinyue L, Xin L, Min L, Weiqing Y, Aigui Z, Zhonghua Q, Menglin M (2026) Investigation of the synthesis and antioxidant activity of novel derivatives of the natural compound daidzein and the quantitative structure–activity relationships. Nat Prod Res 1–7.

[8] Mercieca AL, Alonzo M, Chadwick S, McDonagh AM (2026) Oxidative processes to transform and degrade amphetamine-type stimulants: alternatives to incineration. Drug Test Anal 18(1):96–107.

[9] Samsonowicz M (2014) Molecular structure of phenyl- and phenoxyacetic acids: spectroscopic and theoretical study. Spectrochim Acta A 118:1086–1097.

[10] Srivastava AK, Baboo V, Narayana B, Sarojini BK, Misra N (2014) Comparative DFT study on reactivity, acidity and vibrational spectra of halogen substituted phenylacetic acids. Indian J Pure Appl Phys 52:507–519.

[11] Scalmani G, Frisch MJ, Mennucci B, Tomasi J, Cammi R, Barone V (2006) Geometries and properties of excited states in the gas phase and in solution: theory and application of a time-dependent density functional theory polarizable continuum model. J Chem Phys 124:094107.

[12] Frisch MJ, Trucks GW, Schlegel HB, Scuseria GE, Robb MA, Cheeseman JR, Scalmani G, Barone V, Petersson GA, Nakatsuji H, Li X, Caricato M, Marenich AV, Bloino J, Janesko BG, Gomperts R, Mennucci B, Hratchian HP, Ortiz JV, Izmaylov AF, Sonnenberg JL, Williams-Young D, Ding F, Lipparini F, Egidi F, Goings J, Peng B, Petrone A, Henderson T, Ranasinghe D, Zakrzewski VG, Gao J, Rega N, Zheng G, Liang W, Hada M, Ehara M, Toyota K, Fukuda R, Hasegawa J, Ishida M, Nakajima T, Honda Y, Kitao O, Nakai H, Vreven T, Throssell K, Montgomery JA Jr, Peralta JE, Ogliaro F, Bearpark MJ, Heyd JJ, Brothers EN, Kudin KN, Staroverov VN, Keith TA, Kobayashi R, Normand J, Raghavachari K, Rendell AP, Burant JC, Iyengar SS, Tomasi J, Cossi M, Millam JM, Klene M, Adamo C, Cammi R, Ochterski JW, Martin RL, Morokuma K, Farkas O, Foresman JB, Fox DJ (2016) Gaussian 16, Gaussian Inc., Wallingford CT

[13] Becke AD (1993) A new mixing of Hartree–Fock and local density-functional theories. J Chem Phys 98:1372–1377.

[14] Lee C, Yang W, Parr RG (1988) Development of the Colle–Salvetti correlation-energy formula into a functional of the electron density. Phys Rev B 37:785–789.

[15] Raghavachari K, Binkley JS, Seeger R, Pople JA (1980) Self-consistent molecular orbital methods. 20. Basis set for correlated wave-functions. J Chem Phys 72:650–654.

[16] Gaussian Inc. (2016) GaussView 6.0.16, Wallingford CT

[17] Borba A, Albrecht M, Gomez-Zavaglia A, Lapinski L, Nowak MJ, Suhm MA, Fausto R (2008) Dimer formation in nicotinamide and picolinamide in the gas and condensed phases probed by infrared spectroscopy. Phys Chem Chem Phys 10:7010–7021.

[18] Koopmans T (1934) Über die Zuordnung von Wellenfunktionen und Eigenwerten zu den einzelnen Elektronen eines Atoms. Physica 1:104–113.

[19] Janak JF (1978) Proof that $\partial E/\partial n_i = \varepsilon_i$ in density-functional theory. Phys Rev B 18:7165–7168.

[20] Perdew JP, Levy M (1983) Physical content of the exact Kohn–Sham orbital energies: band gaps and derivative discontinuities. Phys Rev Lett 51:1884–1887.

[21] Pearson RG (1986) Absolute electronegativity and hardness correlated with molecular orbital theory. Proc Natl Acad Sci USA 83(22):8440–8441.

[22] Parr RG, Szentpaly LV, Liu S (1999) Electrophilicity index. J Am Chem Soc 121(9):1922–1924.

[23] Gazquez JL, Cedillo A, Vela A (2007) Electrodonating and electroaccepting powers. J Phys Chem A 111(10):1966–1970.

[24] Gomez B, Likhanova NV, Domínguez-Aguilar MA, Martínez-Palou R, Vela A, Gazquez JL (2006) Quantum chemical study of the inhibitive properties of 2-pyridyl-azoles. J Phys Chem B 110(18):8928–8934.

[25] Foster JP, Weinhold F (1980) Natural hybrid orbitals. J Am Chem Soc 102(24):7211–7218.

[26] Reed AE, Weinhold F (1985) Natural localized molecular orbitals. J Chem Phys 83:1736–1740.

[27] Daina A, Michielin O, Zoete V (2014) iLOGP: a simple, robust, and efficient description of n-octanol/water partition coefficient for drug design using the GB/SA approach. J Chem Inf Model 54(12):3284–3301.

[28] Cheng T, Zhao Y, Li X, Lin F, Xu Y, Zhang X, Li Y, Wang R (2007) Computation of octanol–water partition coefficients by guiding an additive model with knowledge. J Chem Inf Model 47(6):2140–2148.

[29] Wildman SA, Crippen GM (1999) Prediction of physicochemical parameters by atomic contributions. J Chem Inf Comput Sci 39(5):868–873.

[30] Lipinski CA, Lombardo F, Dominy BW, Feeney PJ (2001) Experimental and computational approaches to estimate solubility and permeability in drug discovery and development settings. Adv Drug Deliv Rev 46:3–26.

[31] https://https://www.swissadme.ch/

[32] Delaney JS (2004) ESOL: estimating aqueous solubility directly from molecular structure. J Chem Inf Comput Sci 44(3):1000–1005.

[33] Ali J, Camilleri P, Brown MB, Hutt AJ, Kirton SB (2012) In silico prediction of aqueous solubility using simple QSPR models: the importance of phenol and phenol-like moieties. J Chem Inf Model 52(11):2950–2957.

[34] Ghose AK, Viswanadhan VN, Wendoloski JJ (1999) A knowledge-based approach in designing combinatorial or medicinal chemistry libraries for drug discovery. 1. A qualitative and quantitative characterization of known drug databases. J Comb Chem 1(1):55–68.

[35] Veber DF, Johnson SR, Cheng HY, Smith BR, Ward KW, Kopple KD (2002) Molecular properties that influence the oral bioavailability of drug candidates. J Med Chem 45(12):2615–2623.

[36] Egan WJ, Merz KM Jr, Baldwin JJ (2000) Prediction of drug absorption using multivariate statistics. J Med Chem 43(21):3867–3877.

[37] Muegge I, Heald SL, Brittelli D (2001) Simple selection criteria for drug-like chemical matter. J Med Chem 44(12):1841–1846.

[38] Martin YC (2005) A bioavailability score. J Med Chem 48(9):3164–3170.

[39] Daina A, Michielin O, Zoete V (2017) SwissADME: a free web tool to evaluate pharmacokinetics, druglikeness and medicinal chemistry friendliness of small molecules. Sci Rep 7:42717.

[40] Daina A, Zoete V (2016) A BOILED-Egg to predict gastrointestinal absorption and brain penetration of small molecules. ChemMedChem 11(11):1117–1121.